Iterative Jacobian-Based Inverse Kinematics and Open-Loop Control of an MRI-Guided Magnetically-Actuated Steerable Catheter System

Taoming Liu, Russell Jackson, Dominique Franson, Nate Lombard Poirot, Reinhardt Kam Criss, Nicole Seiberlich, Mark A. Griswold, M. Cenk Çavuşoğlu

***Abstract*—This paper presents an iterative Jacobian-based inverse kinematics method for an MRI-guided magnetically-actuated steerable intravascular catheter system. The catheter is directly actuated by magnetic torques generated on a set of current-carrying micro-coils embedded on the catheter tip, by the magnetic field of the magnetic resonance imaging (MRI) scanner. The Jacobian matrix relating changes of the currents through the coils to changes of the tip position is derived using a three dimensional kinematic model of the catheter deflection. The inverse kinematics is numerically computed by iteratively applying the inverse of the Jacobian matrix. The damped least square method is implemented to avoid numerical instability issues that exist during the computation of the inverse of the Jacobian matrix. The performance of the proposed inverse kinematics approach is validated using a prototype of the robotic catheter by comparing the actual trajectories of the catheter tip obtained via open-loop control with the desired trajectories. The results of reproducibility and accuracy evaluations demonstrate that the proposed Jacobian-based inverse kinematics method can be used to actuate the catheter in open-loop to successfully perform complex ablation trajectories required in atrial fibrillation ablation procedures. This study paves the way for effective and accurate closed-loop control of the robotic catheter with real-time feedback from MRI guidance in subsequent research.**

***Index Terms*—Robotic Catheter, Magnetically Actuated Catheter, Continuum Robots, Inverse Kinematics.**

I. Introduction

CATHETER ablation (Fig. 1(a)) is a widely performed minimally invasive procedure for treatment of atrial fibrillation [1, 2]. For the last decade, robotic catheters have emerged as a promising technology for catheter ablation. A physician can remotely steer the catheter while seated comfortably in the control room and be safely protected from radiation. The catheter is guided by the physician to the left atrium via passing through the femoral vein, the right atrium and the atrial septal wall (Fig. 1(a)). In the left atrium, the tip is steered to reach the desired area, such as ostia of pulmonary veins (Fig. 1(a)), and radiofrequency energy is applied to form barriers to prevent the spread of irregular electrical signals.

So far, two robotic catheter systems received U.S. Food and Drug Administration (FDA) clearances, the Niobe™ ES magnetic navigation system [4] (Stereotaxis, St. Louis, MO) for the atrial fibrillation ablation and the Magellan™ robotic system [5] (Hansen Medical, Mountain View, CA) for the advanced endovascular procedures. The advantages of using robotic catheters include less physical demand on physicians, lower radiation exposure, greater catheter stability, higher reproducibility, better catheter control and improved procedural predictability and safety in ablation treatments [6].

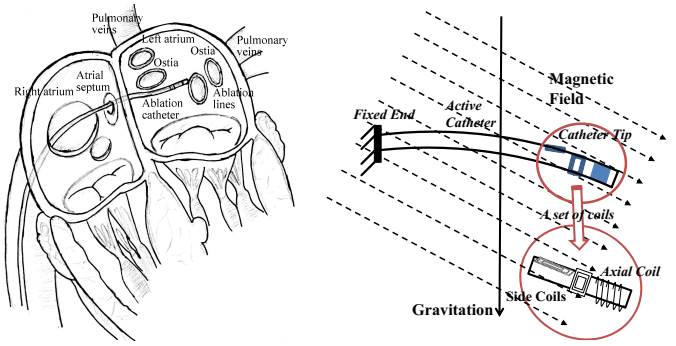

(a) (b)

Fig. 1: (a) Illustration of catheter ablation procedure [3]. (b) Illustration of a proof-of-concept catheter prototype in a magnetic field, including a set of embedded current-carrying coils [3].

Magnetic resonance imaging (MRI) is a promising imaging method for cardiac ablation procedures due to its superior soft-tissue visualization with no radiation exposure [7, 8]. MRI has been used both pre-procedurally to gather detailed anatomical information of the left atrium and related areas, and post-procedurally to detect complications and to visualize lesions [9]. Real-time catheter guidance and lesion visualization using MRI has also been demonstrated [7–9]. Additionally, the MRI scanner can directly provide actuation torques to robotic catheters. Muller et al. reviewed different remote control catheter navigation approaches under MRI [10]. Designs of magnetically-actuated catheters were proposed in [11–18]. The catheter is embedded with a set of current-carrying coils [11, 13, 14], or a set of beads made of ferromagnetic materials [15], or a set of magnets [16–18]. In [11, 13], the catheter is remotely steered by passing currents through the coils which generate magnetic torques in the magnetic field of MRI scanner. In [15, 16], the catheter is deflected by changing the gradients of the MRI scanner which generate magnetic forces on the ferromagnetic components.

This paper proposes a Jacobian-based inverse kinematics method to control the deflection of a catheter, which is embedded with a set of electromagnetic coils on its tip. The

*This work was supported in part by National Science Foundation under grants CISE IIS-1524363 and IIS-1563805, and National Institutes of Health under grant R01 EB018108.

All authors are with Case Western Reserve University, Cleveland, Ohio 44106, USA. T. Liu, R. Jackson, R. K. Criss and M. C. Çavuşoğlu are with the Department of Electrical Engineering and Computer Science. N. L. Poirot is with the Department of Mechanical and Aerospace Engineering. D. Franson, N. Seiberlich and M. A. Griswold are with the Department of Biomedical Engineering. M. A. Griswold is also with the Department of Radiology, University Hospitals of Cleveland, Cleveland, Ohio 44106, USA (Email: {txl168, rcj33, dnf7, njl49, rarity, nes30, mcc14, mag46}@case.edu).

catheter is directly actuated by the magnetic torques generated by the magnetic field of the MRI scanner on these coils (Fig. 1(b)), by controlling the amount of current going through the coils. In such a scenario, the catheter system is not subject to the mechanical transmission problems that exist in other actuation methods (such as tendon-driven [5] and hydraulic [19] actuation) which place the actuators outside the patient body. This magnetic actuation method reduces backlash and friction in the system. As accurate control of the catheter tip position is a critical performance requirement for ablation procedures [2, 20], the proposed catheter system will help the physicians by facilitating them to easily control the catheter motions and to precisely move the catheter tip to the desired targets on the atrial wall [2, 20].

For the proposed catheter system, the Jacobian matrix, which relates changes of the currents through the coils (system input) to changes of the tip position (system output), is derived from a three dimensional model proposed by Liu et al. [3, 21]. The inverse kinematics method is implemented using the damped least squares method [22–24] which avoids stability problems in the neighborhood of singularities that exist in the Jacobian matrix. The performance of the proposed inverse kinematics approach is validated using a prototype of the robotic catheter by comparing the actual trajectories of the catheter tip obtained via open-loop control with the desired trajectories. A camera-based vision system is used to track the catheter deflections in the experiments.

Related studies in the literature regarding control of the robotic catheters are discussed in Section II. A review of the kinematic model of the catheter and the derivation of the Jacobian are presented in Section III. The inverse kinematics method is described in Section IV. The experimental set-up and procedures are described in Section V. The experimental results are presented in Section VI, followed by the discussions and conclusions in Sections VII and VIII.

II. Related Studies

Robotic catheters are redundant continuum robots with infinite degrees-of-freedom (DoF) [25]. The computation of their inverse kinematics, which maps from task space to configuration space, is challenging due to the highly nonlinear nature of this mapping. The state-of-the-art methods for the solution of continuum robot inverse kinematics can be broadly categorized into geometric and differential kinematic (Jacobian-based) approaches, as discussed in the recent survey articles [25] and [26].

Neppalli et al. [27] proposed a geometric approach for solving the inverse kinematics of a single-section trunk under the assumption of constant curvature, and then extended this method to multiple sections by assuming knowledge of end-point locations on these sections and compensating orientations of these sections. This approach assumed that gravity loading had no deformation effects on the sections and did not account for physical actuation limits.

The Jacobian-based approach is a common method for solving inverse kinematics of redundant robotic manipulators. Siciliano [28] published a tutorial introducing several online instantaneous control methods for kinematic control. The Jacobian of the manipulator plays an important role in these methods. Although this tutorial mainly focuses on rigid-link robots, the methods are also applicable to continuum robots.

Gravagne et al. [29] proposed a large-deflection dynamics model for planar continuum robots and developed a PD-plus-coupling setpoint control strategy. Then later, Jones and Walker [30] proposed a Jacobian-based method to control pneumatically-actuated (or tendon-driven) multi-section continuum robots. The method relates cartesian coordinates of the manipulator to actuator inputs via robot shape coordinates. In [31], they extended the method to take into account actuator length limits and cable tangling/untangling effects for practical and effective control of continuum robots, especially for tendon-driven robots.

Camarillo et al. [32, 33] developed a linear beam configuration model for tendon-driven catheter robots. This model transforms beam configurations to tendon displacements and also relates tendon displacements to tendon forces. In order to control the catheter in configuration and task spaces, while avoiding tendon slack issues, the authors optimized the actuation loads by considering the tendon slack constraints together with the kinematics and the Jacobian. Yip and Camarillo [34] proposed a model-less feedback position control scheme for catheter manipulation in constrained environments. In this method, the controller continually updates an estimated Jacobian, which relates incremental actuation to end effector displacements, using end-effector position measurements. Recently, they extended the method to the model-less hybrid position/force control using end-effector position and force measurements [35, 36].

In [11, 13, 14], deflections of a magnetic micro-catheter was modeled using beam theory. The whole catheter was modeled as a cantilever beam, such that the magnetic torque generated on the solenoid is equal to the torque of the whole beam attempting to return to the initial state. This approach works for a catheter prototype with one three-axis coil rather than multiple three-axis coils. Tunay developed a closed-loop position control system of a magnetically-actuated catheter embedding a permanent magnet near the distal tip [37], used in the Stereotaxis system [4]. The inverse of the Jacobian matrix of output and the decoupled and linear error dynamics were used to compute the necessary control effort.

Simaan et al. [38] developed a Jacobian for a multi-backbone continuum robot and Bajo et al. [39] employed the Jacobian to implement configuration-space and task-space controls of continuum robots using both extrinsic and intrinsic sensory information.

Concentric-tube robots, comprised of multiple precurved elastic tubes, are another interesting research topic in continuum robots. In these systems, the robot tip is moved by rotations and insertions of these precurved tubes with respect to each other. Dupont et al. [40] achieved real-time control of a concentric-tube robot by precomputing approximations of the forward kinematics with torsion and employing the Jacobian-inverse approach with Newton's root-finding method. Webster [41] developed a Jacobian-based visual servo controller for locating the tip of the concentric-tube continuum robot. Later, Rucker and Webster [42] adopted a generalized damped least-

square approach with Jacobian and compliance matrices for modeling externally loaded continuum robots. In order to achieve the practical use of the concentric robots in real-time, Xu et al. [43] developed an efficient modified Jacobian approach based on the kinematics proposed by Dupont et al. [40] for position control. Boushaki et al. [44] used approximate Jacobian for task-space position control of a concentric-tube robot with inaccurate kinematics.

Most of the previous literature on kinematics and control of continuum robots primarily focused on tendon-driven continuum robots and concentric-tube robots, where the actuation is located on the proximal end. In this paper, we present Jacobian-based inverse kinematics of an MRI-actuated steerable catheter and validate the proposed method using open loop control in hardware experiments. This study paves the way for effective and accurate closed-loop control of the robotic catheter with real-time feedback from MRI guidance for the treatment of atrial fibrillation in subsequent research. Although outside the scope of the current paper, the presented Jacobian-based scheme can also be used as part of a doctor-in-the-loop teleoperation control paradigm for controlling the catheter (e.g., [5, 45, 46]).

III. Differential Kinematics

A. Catheter Actuation

In the proposed scheme, the catheter is embedded with one or multiple coil sets along the body. Each coil set includes one axial coil and two orthogonal coils (as shown in Fig. 1(b)). In a magnetic field, magnetic torques can be generated on these coils by passing through currents. This allows the control of the catheter's three dimensional deflection by controlling the currents. The direction and amplitude of the magnetic torque are determined by the cross product of the magnetic moment from each coil and the magnetic field. The workspace of the proposed catheter with multiple coil sets is analyzed for optimization of the catheter design by Liu et al. [47].

B. Review of Forward Kinematics

Liu et al. [3, 21] developed a method combining a finite differences approach with beam theory and rotation groups to model the proposed MRI-actuated catheter's three dimensional deflection motion, including bending and torsion. There are some earlier studies where Cosserat rod theory is applied to model continuum robots (e.g., [17, 48]). The main advantage of the employed formulation [3, 21] is that it is easy to incorporate external forces and torques on the tip or along the catheter body, which is essential for calculating deflections under multi-coil actuation. In this paper, a Jacobian-based inverse kinematics method for control of the steerable catheter based on the proposed model [3, 21] is developed.

In the kinematic model presented in [3, 21], the catheter is approximated to be composed of a set of finite segments[1] (shown in Fig. 2). The deflection of each segment is assumed to have two small bending angles and one torsion angle.

[1]The number of segments to discretize the catheter is a constant in the current method. A discussion of choosing this number is presented in [21].

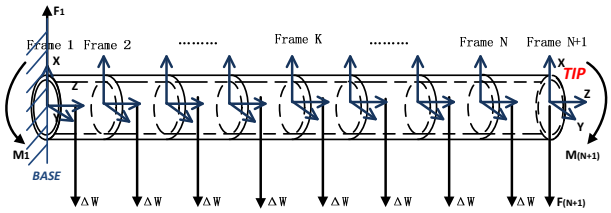

Fig. 2: Diagram of a catheter with one set of current-carrying coils, which is divided into N finite segments [3]. The coil is located at the tip.

The deflection of an individual segment is solved using beam theory and the Bernoulli-Euler law. Considering each segment as a flexible robot link with constant curvature, a homogeneous transformation relationship between the two ends is calculated by using the computed deflection and torsion angles. Using these, the homogeneous transformation between any two points on any two segments can be found. The force/torque equilibrium equations for each of the segments are then set up based on each segment's deflection angles.

The equilibrium equations for the K^{th} segment ($K \in \{1, \cdots, N\}$) are

$$\begin{aligned} M_K &= R_{K,K+1}M_{K+1} + P_{K,K+1} \times (R_{K,K+1}F_{K+1}) + \\ &\qquad Q_{K,K+1} \times (R_{K,1}\triangle W_K), \\ F_K &= R_{K,K+1}F_{K+1} + R_{K,1}\triangle W_K, \end{aligned} \tag{1}$$

where the M_{K} and F_{K} (K$\in \{1, \cdots, \mathrm{N}\}$) represent the torque and force vectors acting on the K^{th} segment, vector ΔW_K represents the weight of the segment, $P_{K,K+1}$ and $Q_{K,K+1}$ represent the end point and the center of the K^{th} segment in frame K coordinates, and, $R_{K,K+1}$ represents the rotation matrix between two ends on the K^{th} segment. The resulting deflection of each segment (K $\in \{1, \cdots, \mathrm{N}\}$) is given by

$$S_K \cdot M_K = C_K \cdot X_K, \tag{2}$$

where, X_K represents the vector of deflection and torsion angles of the K^{th} segment, S_K represents a matrix including the area moments of inertia and the area product of inertia of the K^{th} segment cross section, C_K represents the stiffness matrix of the K^{th} segment considering the material properties (such as Young's modulus and shear modulus). The specific details of the deflection model are explained in [3, 21].

The magnetic torque $M_{\mathrm{N+1}}$ from the electromagnetic coils embedded on the catheter tip, is given by:

$$M_{\mathrm{N+1}} = \overrightarrow{\mu_{\mathrm{N+1}}} \times (R_{N+1,1}B_{0,1}), \tag{3}$$

where the vector $B_{0,1}$ represents the main (B_0) magnetic field of the MRI system relative to the base frame[2], and the $\overrightarrow{\mu_{\mathrm{N+1}}}$ represents the total magnetization vector of the catheter coils relative to frame $N+1$, which can be expressed as:

$$\overrightarrow{\mu_{\mathrm{N+1}}} = V_x \mathrm{i}_x A_x \overrightarrow{\mu_x} + V_y \mathrm{i}_y A_y \overrightarrow{\mu_y} + V_z \mathrm{i}_z A_z \overrightarrow{\mu_z}. \tag{4}$$

[2]$B_{0,1}$ refers to the constant, homogeneous magnetic field used to polarize spins, creating magnetization in MRI scanner. This magnetic field is customarily referred to as the B_0 field in the MRI literature, and the subscript 1 represents that this vector is expressed relative to the coordinate frame defined on the catheter base.

V_j represents the number of turns in the coil j, A_j is the area enclosed by each turn of the coil j, and i_j is the current through the coil j. For simplicity, (3) can be transformed to

$$M_{\mathrm{N+1}} = -(R_{N+1,1}B_{0,1})^{\wedge}(\mathbf{Vi}), \tag{5}$$

where

$$\mathbf{V} = \begin{bmatrix} V_x A_x & 0 & 0 \\ 0 & V_y A_y & 0 \\ 0 & 0 & V_z A_z \end{bmatrix},$$

and

$$\mathbf{i} = \begin{bmatrix} \mathrm{i}_x & \mathrm{i}_y & \mathrm{i}_z \end{bmatrix}^{\mathrm{T}}.$$

C. Jacobian

In the system, the differential kinematics (Jacobian) represents the relationship between the infinitely small changes of the catheter tip position and the coil currents:

$$\mathbf{J} = \frac{d\mathbf{P}}{d\mathbf{i}}. \tag{6}$$

Since a closed form expression for the catheter tip position $\mathbf{P}$ as a function of the coil currents $\mathbf{i}$ is not available, it is not possible to directly calculate (6). However, the Jacobian can be computed using the chain rule as

$$\mathbf{J} = \frac{d\mathbf{P}}{d\mathbf{X}} \cdot \frac{d\mathbf{X}}{d\mathbf{i}}, \tag{7}$$

since the relationship between the changes in the deflection angles $d\mathbf{X}$ and the currents $d\mathbf{i}$ is available in closed form. Therefore, the calculation of Jacobian is divided into two parts, namely, the calculation of $\frac{d\mathbf{X}}{d\mathbf{i}}$ and $\frac{d\mathbf{P}}{d\mathbf{X}}$.

1) Calculation of $\frac{d\mathbf{X}}{d\mathbf{i}}$: Noting that the catheter coils only exert external moments to segment N, and the equation for M_K depends only on segment orientations $X_1, \cdots, X_{k+1}$, (1) and (5) can be rearranged into the following forms by representing the torque of each segment as a function of the coil currents $\mathbf{i}$ and the orientation angles $\mathbf{X}$:

$$\begin{array}{rcl} M_{\mathrm{N+1}} & = & f_{\mathrm{N+1}}(\mathbf{i}, \mathbf{X}_1, \cdots, \mathbf{X}_{\mathrm{N}}), \\ M_{\mathrm{N}} & = & f_{\mathrm{N}}(\mathbf{i}, \mathbf{X}_1, \cdots, \mathbf{X}_{\mathrm{N}}), \\ M_{\mathrm{N\text{-}1}} & = & f_{\mathrm{N\text{-}1}}(0, \mathbf{X}_1, \cdots, \mathbf{X}_{\mathrm{N}}), \\ \vdots & \vdots & \vdots \\ M_{\mathrm{K}} & = & f_{\mathrm{K}}(0, \mathbf{X}_1, \cdots, \mathbf{X}_{\mathrm{k+1}}, 0, \cdots, 0), \\ \vdots & \vdots & \vdots \\ M_1 & = & f_1(0, \mathbf{X}_1, \mathbf{X}_2, 0, \cdots, 0). \end{array} \tag{8}$$

As $M_{\mathrm{N+1}}$ is a function of $\mathbf{i}$ in (5) and M_{N} is related to $M_{\mathrm{N+1}}$, M_{N} is also a function of $\mathbf{i}$. Differentiating (8) with respect to $\mathbf{i}$ using the chain rule and rearranging it appropriately yields the following equation:

$$\begin{bmatrix} A_{1,1} & A_{1,2} \\ A_{2,1} & A_{2,2} \end{bmatrix} \begin{bmatrix} \frac{dM_{N+1}}{d\mathbf{i}} \\ \frac{d\mathbf{X}}{d\mathbf{i}} \end{bmatrix} = \begin{bmatrix} E_{1,1} \\ E_{2,1} \end{bmatrix}, \tag{9}$$

where the block matrices are $A_{1,1} = -I_{3\times3}$, $E_{1,1} = -\frac{\partial f_{N+1}}{\partial \mathbf{i}}$,

$$A_{1,2} = \begin{bmatrix} \frac{\partial f_{N+1}}{\partial \mathbf{X}_1} & \frac{\partial f_{N+1}}{\partial \mathbf{X}_2} & \frac{\partial f_{N+1}}{\partial \mathbf{X}_3} & \cdots & \frac{\partial f_{N+1}}{\partial \mathbf{X}_{N\ 1}} & \frac{\partial f_{N+1}}{\partial \mathbf{X}_N} \end{bmatrix},$$

$$A_{2,1} = \begin{bmatrix} 0_{3\times3} & 0_{3\times3} & \ldots & 0_{3\times3} \end{bmatrix}^T,$$

$$E_{2,1} = \begin{bmatrix} -\frac{\partial f_N}{\partial \mathbf{i}} & 0_{3\times3} & \ldots & 0_{3\times3} \end{bmatrix}^T,$$

and, $I_{3\times3}$ and $0_{3\times3}$ denote the 3-by-3 identity matrix and the 3-by-3 zero matrix, individually. In addition, $A_{2,2}$ can be further divided into the sum of two matrices G and H, where

$$G = \begin{bmatrix} \frac{\partial f_N}{\partial \mathbf{X}_1} & \frac{\partial f_N}{\partial \mathbf{X}_2} & \frac{\partial f_N}{\partial \mathbf{X}_3} & \cdots & \frac{\partial f_N}{\partial \mathbf{X}_{N\ 1}} & \frac{\partial f_N}{\partial \mathbf{X}_N} \\ \frac{\partial f_{N\ 1}}{\partial \mathbf{X}_1} & \frac{\partial f_{N\ 1}}{\partial \mathbf{X}_2} & \frac{\partial f_{N\ 1}}{\partial \mathbf{X}_3} & \cdots & \frac{\partial f_{N\ 1}}{\partial \mathbf{X}_{N\ 1}} & \frac{\partial f_{N\ 1}}{\partial \mathbf{X}_N} \\ \frac{\partial f_{N\ 2}}{\partial \mathbf{X}_1} & \frac{\partial f_{N\ 2}}{\partial \mathbf{X}_2} & \frac{\partial f_{N\ 2}}{\partial \mathbf{X}_3} & \cdots & \frac{\partial f_{N\ 2}}{\partial \mathbf{X}_{N\ 1}} & 0_{3\times3} \\ \vdots & \vdots & \vdots & \vdots & \vdots & \vdots \\ \frac{\partial f_1}{\partial \mathbf{X}_1} & \frac{\partial f_1}{\partial \mathbf{X}_2} & 0_{3\times3} & \cdots & 0_{3\times3} & 0_{3\times3} \end{bmatrix},$$

and

$$H = \begin{bmatrix} 0_{3\times3} & 0_{3\times3} \cdots & 0_{3\times3} & -S^{-1}C \\ 0_{3\times3} & 0_{3\times3} \cdots & -S^{-1}C & 0_{3\times3} \\ \vdots & \vdots & \vdots & \vdots \\ -S^{-1}C & 0_{3\times3} \cdots & 0_{3\times3} & 0_{3\times3} \end{bmatrix}.$$

As the block $A_{2,1}$ is a zero matrix, $\frac{d\mathbf{X}}{d\mathbf{i}}$ can be computed as

$$\frac{d\mathbf{X}}{d\mathbf{i}} = A_{2,2}^{-1} \cdot E_{2,1} = (G+H)^{-1} \cdot E_{2,1}. \tag{10}$$

As the orientation angles for each segment q are in the form

$$\mathbf{X}_q = \begin{bmatrix} \theta_{q,x} & \theta_{q,y} & \theta_{q,z} \end{bmatrix}^T,$$

each term in the G matrix can be calculated as follows:

$$\frac{\partial f_p}{\partial \mathbf{X}_q} = \begin{bmatrix} \frac{\partial f_p}{\partial \theta_{q,x}} & \frac{\partial f_p}{\partial \theta_{q,y}} & \frac{\partial f_p}{\partial \theta_{q,z}} \end{bmatrix},$$

where $p \in \{1, \cdots, N\}$, and $q \in \{1, \cdots, N\}$.

2) Calculation of $\frac{d\mathbf{P}}{d\mathbf{X}}$: The kinematic model of each segment can be treated as a 3 DoF flexible robotic link with constant curvature and solved as a differential equation with respect to arc length along the centerline of the catheter segment [49, 50]. Therefore, the tip position of the $(N+1)^{th}$ segment in the base frame, which is the position of the catheter tip, can then be calculated as

$$\mathbf{P} = e^{\hat{\xi}_{1,\,2}\,s} e^{\hat{\xi}_{2,\,3}\,s} \ldots e^{\hat{\xi}_{\mathrm{N},\,\mathrm{N+1}}\,s} \begin{bmatrix} 0 & 0 & 0 & 1 \end{bmatrix}^{\mathrm{T}}, \tag{11}$$

where $e^{\hat{\xi}_{\mathrm{i},\,\mathrm{i+1}}\,s}$ is the coordinate transformation between the i^{th} and $(i+1)^{th}$ segment [3, 21]. Then

$$\frac{d\mathbf{P}}{d\mathbf{X}} = \begin{bmatrix} \frac{d\mathbf{P}}{d\theta_x} & \frac{d\mathbf{P}}{d\theta_y} & \frac{d\mathbf{P}}{d\theta_z} \end{bmatrix} \tag{12}$$

can be explicitly calculated in a straightforward manner.

IV. Inverse Kinematics

Inverse kinematics is frequently used in control of robotic manipulation. Here, the goal is to find the coil currents required to achieve a given catheter tip position. Closed-form solution of the inverse kinematics is not possible because of the complexity of the kinematics. Therefore, a Jacobian-based numerical method is implemented.

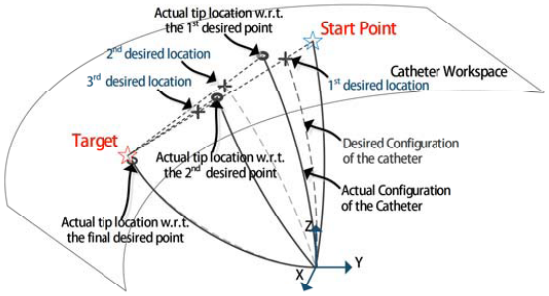

Fig. 3: An illustration of the iterative inverse kinematics method.

A. Jacobian-based method

There are several methods for solving inverse kinematics problems numerically. Jacobian-based methods are commonly used for numerically solving the inverse kinematics problem. The Jacobian (6) derived in the previous section relates incremental changes in the input currents to incremental changes in the tip position. (6) can be rearranged to give

$$d\mathbf{P} = \mathbf{J}d\mathbf{i}. \tag{13}$$

If the desired displacement ($d\mathbf{P}$) is small, a linear approximation can be used to calculate the necessary change in coil currents ($d\mathbf{i}$) to achieve a given tip displacement using the inverse of the Jacobian.

However, this typically would not be practical, since Jacobian may not be invertible or may be ill-conditioned. Therefore, the quality of the inverse kinematics depends on the representation of the inverse of the Jacobian. As it can be observed from the computation in Section III, the Jacobian of the catheter system is always singular. Greigarn and Cavusoglu [51] has analyzed the singularities in the joint and task spaces. Therefore, the damped least square method, which avoids this stability issue [22–24], is appropriate to solve the inverse kinematics of the catheter system considered. Specifically,

$$d\mathbf{i} = \mathbf{J}^T(\mathbf{J}\mathbf{J}^T + \lambda^2\mathbf{I}_{3\times3})^{-1}d\mathbf{P}, \tag{14}$$

where λ is a non-zero damping constant. Here, λ is 0.01. For simplifying the process, the singular decomposition method (SVD) is used to calculate $\mathbf{J}^T(\mathbf{J}\mathbf{J}^T + \lambda^2\mathbf{I}_{3\times3})^{-1}$ in [23, 24].

B. Iterative Inverse Kinematics

As the Jacobian in (13) only relates small changes of the tip position to small changes of the current, directly using the Jacobian in the computation of the inverse kinematics will not lead to accurate results when the starting position of the tip is far away from the goal position.

The approach implemented in this paper is to linearly interpolate multiple points on the direct path which connects the starting position and the target (illustrated in Fig. 3). This would ensure that the position change between the starting position and the first interpolated point, which is closer to the starting position, is appropriately small. In this paper, we do not consider obstacles on the path, as designing advanced path planning algorithms is not within the scope of this paper.

In an example shown in Fig. 3, the Jacobian-based method can be used to compute the currents which allow the catheter to achieve the 1^{st} desired location from the start point. The first step of the motion is

$$d\mathbf{P}_1 = \frac{P_{start} - P_{target}}{K}, \tag{15}$$

where K is the predefined number of steps for the catheter to reach the neighberhood of the target. When this current is actually used for actuation, the actual tip location computed using forward kinematics will end up at a location in the neighborhood of the 1^{st} desired location. Then the linear interpolation approach can be implemented on the path which connects the 1^{st} actual tip location and the target, for obtaining the 2^{nd} desired location. Then the second step of the motion can be calculated as

$$d\mathbf{P}_2 = \frac{P_{now} - P_{target}}{K-1}. \tag{16}$$

The Jacobian-based method can then be used to calculate the currents again. This process can be iteratively repeated for a fixed resolution, or until a desired accuracy is achieved.

V. Experimental Methods

The proposed inverse kinematics method for the MRI-actuated catheter system was validated in hardware experiments. In these experiments, the prototype was driven in open-loop control fashion (without using any sensory feedback of catheter's position) to follow a series of trajectories by using control currents calculated using (14). The resulting motion of the catheter was measured using an external camera and catadioptric stereo tracking, and was evaluated for accuracy and reproducibility. This section describes the experimental setup and the methods. The results are reported in Section VI.

A. Experimental Setup

The experiments were conducted in a 3T clinical scanner (Skyra, Siemens Medical Solutions, Erlangen, Germany), as shown in Fig. 4(a). The front view of the experimental setup is shown in Fig. 4(b). The catheter prototype is mounted vertically inside an aquarium tank (25.4 cm × 25.4 cm × 26.7 cm) and immersed in a phantom filled with distilled water doped with a gadolinium-based contrast agent. The aquarium tank is centered along the central axis of the MRI scanner, but offset from the isocenter to accommodate a mirror which displays the catheter in side perspective. The mirror is needed because a camera can not capture the side motions of the catheter well from outside the MRI scanner bore.

The cables of the coils are connected to a transconductance amplifier controller which stays outside the MRI room. The controller box sets the coil currents using a microcontroller which communicates with a PC through a USB serial link. In this paper, the coil currents are limited to 300 mA[3].

Before each experiment, an MRI image in a coronal slice was used for determining the alignment quality of the setup with the direction of the B_0 magnetic field.

[3]Hetts et al. [52] found in their experiments that when the current for tip coil activation was less than 300 mA and the excitation time was less than 1 minute in normal carotid flow, there was negligible tissue damage.

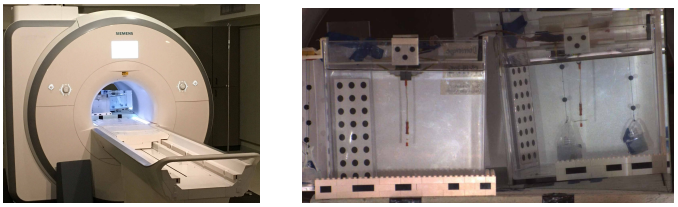

(a) (b)

Fig. 4: (a) Experiment setup inside a clinical MRI scanner. (b) Front view of the experimental setup. The catheter prototype is immersed in a phantom (aquarium tank, left in the picture) filled with distilled water doped with a gadolinium-based contrast agent. It is clamped vertically at its base. The mirror next to the tank (right in the figure) displays the side view of the actuated catheter. The catheter is marked in orange at three spots (base, coils, tip) for measuring the deflections of the catheter prototype using a camera.

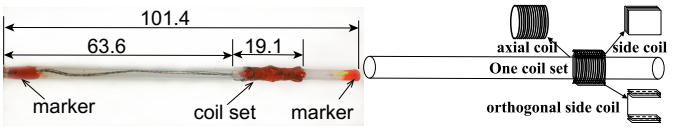

(a) (b)

Fig. 5: (a) A proof-of-concept catheter prototype used in the validation experiments. The unit of the dimensions is in mm. (b) Diagram of the catheter prototype with one coil set. Each coil set is composed of two orthogonal side coils and one axial coil.

B. Description of Catheter Prototype

The catheter prototype (shown in Fig. 5) is embedded with one current-carrying coil set, which includes one 100-turn axial coil and two 30-turn orthogonal side coils. The coils are made of heavy insulated 38-gauge enameled copper wires (Adapt Industries, LLC, Salisbury, MD). They are built over silicone tubing (Part number: T2011, QOSINA, Edgewood, NY). The outer diameter of the tubing is 3.2 mm and the inner diameter is 2.0 mm. The resulting length of the catheter is 101.4 mm. The outer diameter of the catheter prototype, including the coils, is around 3.8 mm. The width of the side coil is 5.1 mm. The length of the coil set is 19.1 mm. The mass of the whole catheter prototype is 1.2 gram.

For measuring the deflections of the catheter prototype using a camera-based vision system, three spots on the catheter (base, coils, tip) are marked in orange as shown in Fig. 5. The lengths of the labeled markers on the base and tip are 6.4 mm and 6.0 mm, respectively.

The catheter deflections were then measured using a catadioptric stereo system. Specifically, a single camera equipped with a zoom lens located outside the MRI scanner bore was used to capture a stereo image created using a mirror which provided a supplemental side view to the front view directly visible to the camera (Fig. 4 (b)). The details of the catadioptric stereo system is available in [53].

C. Estimation of Material Properties

Estimation of catheter deflection using the model presented in Section III-B requires the mechanical parameters of the catheter material. The tubing material used for manufacturing the catheter is silicone. However, the manufacturer only provided a relatively large range for the mechanical parameters, not their specific values. Therefore, the mechanical parameter values of the catheter material are estimated using experimental deflection data.

The mechanical properties of silicon-based polymer material are summarized in [54]. The ranges of Young's modulus, density, and shear modulus are from 1 MPa to 50 MPa, from 1100 kg/m^3 to 2300 kg/m^3, and from 0.3 MPa to 20 MPa, respectively. The density of the tubing material was measured to be approximately 1120 kg/m^3, as it is made of a homogeneous material. As the prototype carries three coils, and the wires for these coils pass through the inner lumen of the catheter to connect to the current source, all of these factors will affect the ultimate flexural rigidity of the catheter together with the material of the tubing. The model approximates the catheter prototype to have uniform flexural rigidity along the shaft. Given these observations and the large ranges of the Young's modulus and shear modulus provided (covering a 50x $\sim$ 70x range), it is necessary to experimentally estimate the values of the Young's modulus and the shear modulus.

D. Open-Loop Control Experiments

Four distinct trajectories (lemniscate, circle, rectangle, and butterfly) are used for evaluating the Jacobian-based inverse kinematics under the open-loop control. The reason for choosing these trajectories is that these shapes are similar to the circumferential and linear ablation lesions employed in atrial fibrillation ablation [2]. The trajectories of the catheter tip are obtained by projecting a 2D geometry shape to the workspace to obtain a list of points on the workspace.

The current corresponding to each point on these trajectories is iteratively calculated using the proposed inverse kinematics method, as explained in Section IV. The calculated currents are applied to actuate the catheter in the experiments. Pause times are artificially introduced in between the trajectory steps in order to acquire multiple camera images at each step, which are averaged to reduce the noise in camera measurements. Experimental data was collected in multiple sessions, each type of trajectory data was collected in a single session.

VI. Results

In this section, the results of the experiments conducted for estimating the Youngs modulus, the shear modulus and the rotation angle of the side coils are presented. Then the experimental performance of the open-loop control of the catheter using the presented method, including reproducibility and accuracy of performing different trajectories are reported.

A. Results of Parameter Estimation

In the experiments for parameter estimation, the catheter was actuated by three series of currents[4]. Fig. 6 shows the observed trajectories of the catheter by actuating the axial coil for bending motion, one side coil for twisting motion, and the

[4]The current values (and the associated experimental data) used for parameter estimation were different from those used in the open-loop control.

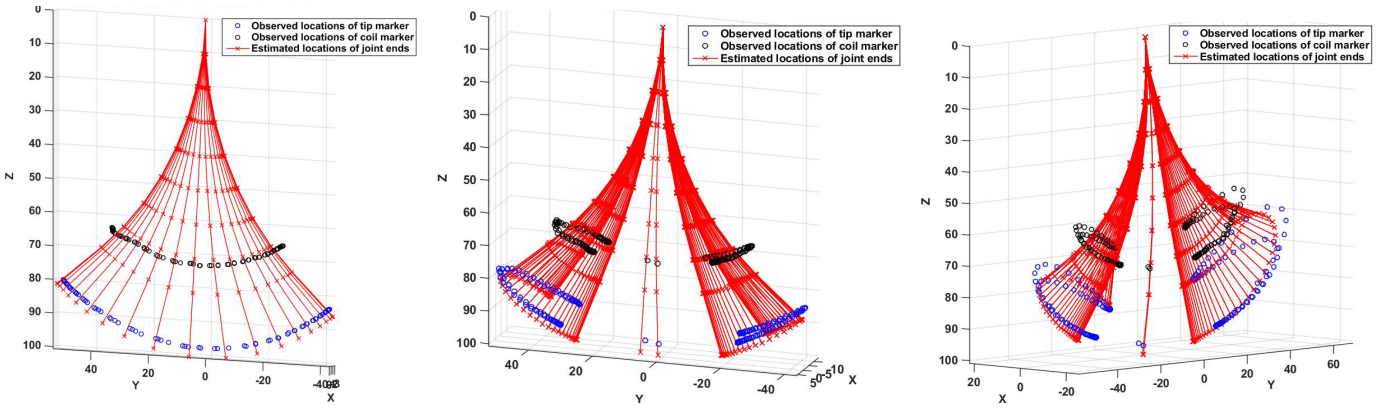

(a) (b) (c)

Fig. 6: Trajectories used for parameter estimations. The blue and black circles show the actual locations of the tip and coil on the catheter. The red stars denote the estimated locations of the end points on each segment of the catheter from the model. (a) Trajectory of the catheter with the axial coil actuated. (b) Trajectory of the catheter with one side coil actuated for twisting motion. (c) Trajectory of the catheter with the other side coil actuated for bending motion.

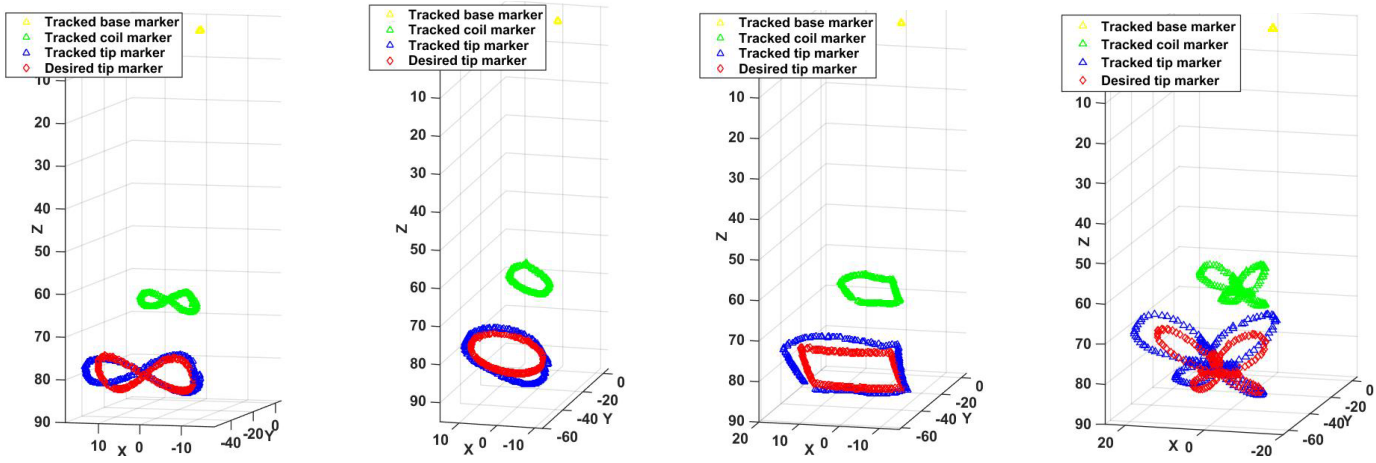

(a) Lemniscate trajectories (b) Circle trajectories (c) Rectangle trajectories (d) Butterfly trajectories

Fig. 7: Catheter trajectories as measured using the camera-based vision system. The red diamonds represent the given trajectories. The blue, green, and yellow squares represent the observed positions of the labeled markers on the tip, coils and base, respectively. The unit in all these plots is mm.

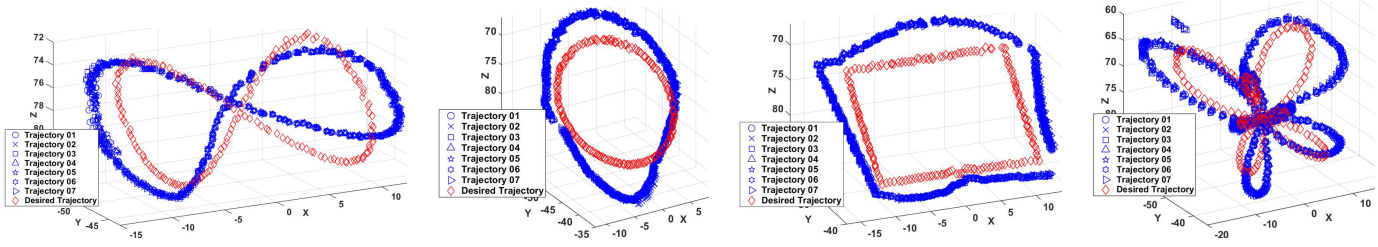

(a) Matched lemniscate trajectories (b) Matched circle trajectories (c) Matched rectangle trajectories (d) Matched butterfly trajectories

Fig. 8: Shape comparisons between the given desired trajectory and the observed trajectories which are transformed without scaling. The red diamonds represent the desired trajectories. The blue markers represent the observed positions of the labeled markers on the tip. Each kind of trajectory has been collected 7 times. The unit in all these plots is mm.

other orthogonal side coil for bending motion, respectively. The blue and black circle markers show the actual locations of the tip and coil on the catheter. The red stars denote the estimated deflection motions of the catheter from the model using the same currents.

These deflection motions were collected for estimating the Young's modulus, shear modulus and the alignment angle of catheter. This angle misalignment is caused by an angular shift between the two orthogonal side coils on the catheter (Fig. 5(b)) and misalignment between the catheter and the direction of the magnetic field when catheter was mounted to tank (Fig. 4(b)). The estimation was performed by minimizing the errors

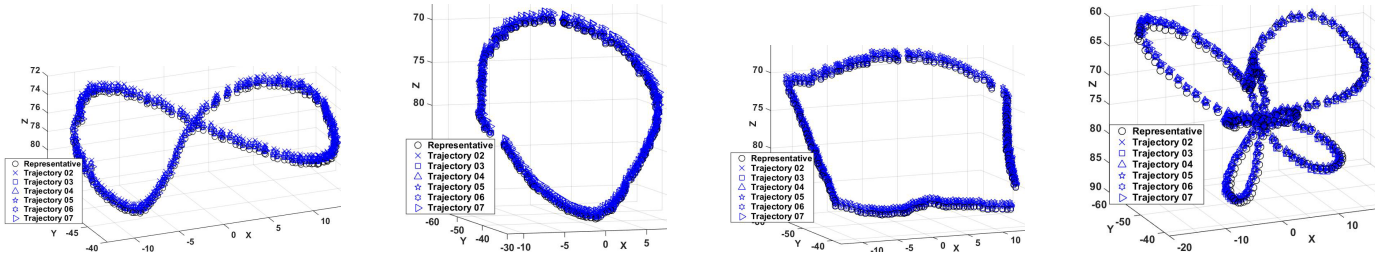

(a) Matched lemniscate trajectories (b) Matched circle trajectories (c) Matched rectangle trajectories (d) Matched butterfly trajectories

Fig. 9: Reproducibility of trajectory shapes among the observed tip trajectories. The black circle markers represent the reference trajectory collected from experiments. The blue markers represent the other observed trajectories of the labeled markers on the tip. Each kind of trajectory has been collected 7 times. The unit in all these plots is mm.

TABLE I: Open-loop trajectory reproducibility performance. In Method 1, the shapes of the observed trajectories were compared to the shape of the given desired trajectory. In Method 2, one of the experimental trajectories were randomly selected as a reference trajectory, and the shapes of the other trajectories were compared to the shape of that reference. The means and variances were calculated from the RMS errors. All units are in mm.

Trajectory	Method 1				Method 2			
	Lemniscate	Circle	Rectangle	Butterfly	Lemniscate	Circle	Rectangle	Butterfly
Mean	1.88	4.11	1.82	3.28	0.35	0.30	0.20	0.54
Variance	0.0089	0.0336	0.0053	0.0320	0.0010	0.0215	0.0043	0.0767
Trial 01	1.86	4.34	1.76	2.94	-	-	-	-
Trial 02	2.05	4.14	1.91	3.30	0.32	0.52	0.13	0.31
Trial 03	1.79	4.34	1.74	3.18	0.34	0.40	0.19	0.88
Trial 04	1.94	3.93	1.79	3.45	0.34	0.10	0.15	0.36
Trial 05	1.77	4.12	1.77	3.31	0.33	0.27	0.19	0.37
Trial 06	1.90	3.96	1.92	3.34	0.41	0.21	0.24	041
Trial 07	1.88	3.91	1.84	3.46	0.34	0.31	0.31	0.91

between the actual deflection and the deflection estimated using the model, including the tip deflection errors and the coil location errors. The estimated values of the Young's modulus, shear modulus, and rotation angle are 5.05 MPa, 1.87 MPa and -25.23^o, respectively.

B. Open-Loop Control Experiment Results

The deflection motions were recorded and tracked by the vision system[5]. Fig. 7 shows the vision-tracked positions of the labeled markers on the catheter (tip marker in blue, coil marker in green and base marker in yellow), which performed the given trajectories represented in red. Each kind of trajectory was performed 7 times during the experiments. There were 200 points along each trajectory. The error between each tip point and the corresponding point captured by the vision system was computed. Then the root-mean-square (RMS) of all these errors on each trajectory was used to quantify the quality of the open-loop control.

As the implemented control is open-loop (which does not use any feedback from measurement of catheter position) and the catheter body is compliant, errors between the given and observed trajectories are expected, shown in Fig. 7. Therefore, shape reproducibility of the trajectories is a more relevant performance metric. However, the overall tracking accuracy of the given trajectories are also reported for completeness.

1) Evaluation of Trajectory Reproducibility: The open-loop trajectory reproducibility was quantified using two methods. In the first method, the shape of the experimentally measured trajectories of the catheter were compared with the shape of the desired motion trajectory. In the second method, one of the measured trajectories was randomly selected as a reference trajectory, and shapes of the other measured trajectories were compared to that reference trajectory. In both methods, the shapes of the trajectories were compared by ignoring position and orientation offsets. Specifically, the trajectories were allowed to be translated and rotated (but not scaled) until the RMS error between them is minimized, and the residual RMS error was used as the shape similarity measure. The resulting reproducibility error is not sensitive to offset (and some drift) types of errors that are inherent to open-loop control schemes, and can easily be eliminated with closed-loop control. The final results are reported in Fig. 8, Fig. 9, and Table I.

Fig. 8 shows the given desired trajectory (red diamonds) and all the observed trajectories (blue markers) after a rigid-body transformation alignments, corresponding to the first method described in the previous paragraph. Fig. 9 shows the shape comparison between the selected reference trajectory (black circles) and all of the other observed trajectories (blue markers), corresponding to the second method. The residual RMS errors between the reference and observed trajectories calculated by both methods are presented in Table I.

The low mean and variance values for the RMS errors indicate very good reproducibility of the trajectory shapes. In other words, the overall shape of the observed trajectory is similar to the corresponding trajectory pattern provided, even for complicated patterns, such as the butterfly pattern.

2) Evaluation of Accuracy: The open-loop trajectory tracking accuracy of the catheter system is reported in Fig. 7 and Table II. The reported RMS error values are in the 3-5

[5]A video attached to this manuscript demonstrates these catheter motions inside the MRI scanner.

TABLE II: Open-loop trajectory accuracy performance. The mean and variance values were calculated from the RMS errors. All units are mm.

	Lemniscate	Circle	Rectangle	Butterfly
Mean	3.25	5.41	3.65	4.87
Variance	0.0037	0.032	0.0026	0.012
Trial 01	3.19	5.54	3.57	4.67
Trial 02	3.31	5.56	3.67	4.90
Trial 03	3.17	5.63	3.60	4.80
Trial 04	3.30	5.25	3.64	4.97
Trial 05	3.19	5.44	3.67	4.89
Trial 06	3.28	5.24	3.71	4.90
Trial 07	3.29	5.19	3.70	4.98

mm range. The smaller reproducibility values (1-4 mm range) reported in the earlier subsection indicate that the trajectory tracking accuracy errors are, in part, due to offset and drift type of errors, and, in part, due to the mismatch of the trajectory shape with respect to the desired trajectory. These errors are typical for open-loop control (and are expected to be eliminated by proper closed-loop control).

VII. Discussions

The computation time of the inverse kinematics is an important concern for clinical applicability of the methods. The computation of applying the Jacobian-based approach per step along the trajectory took approximately 95 ms on a computer equipped with Intel (R) Core (TM) i7-4720HQ CPU @ 2.60 GHz and 8.0 GB memory, running 64-bit Microsoft Windows 8.1 operating system. The algorithms were implemented in Matlab(R) (R2014b) without parallel computing. Significant speedups of the computation time can be expected when all programs are written in C++. It is also possible to construct a look-up table for the workspace for fast on-line operation.

There are several other potential error sources, which may have contributed to the open-loop trajectory accuracy errors. Due to their soft and compliant design, continuum robots can not reach accuracy levels as high as traditional rigid-link robots [30]. There were also small errors resulting from imperfect alignment of the catheter and MRI scanner frames, especially due to variability in mounting of the catheter to the attachment clamp. Although a rotation angle compensating for the shift of the side coils is estimated and used, an accurate alignment between the catheter and the MRI scanner coordinate frames would have improved the performance of the open-loop control of the catheter. Additionally, the workspace that the desired trajectories were computed from used a rest shape of the catheter which was different from the rest configurations of the catheter in different experiments. The specific rest configuration of the catheter in each experiment was not used to update or modify the open-loop current values, since the image processing algorithms used for determining the rest configuration of the catheter were not fast enough for on-line use.

In future work, the MRI scanner will be used to provide the position of the coil on the catheter to the closed-loop controller for real-time image-guided control of the catheter position. The catheter described in this paper can be visualized by taking advantage of the artifact created around the coils mounted on the catheter when they are energized. Typically, the artifact would appear as a signal void (a dark region) surrounding the coils against the standard anatomical image. The detection may be enhanced by using a positive contrast technique in which the catheter instead appears as a bright signal in the image against a dark background [55]. It has been shown that rapid device detection can be achieved by using a projection method similar to that described by Flask et al. [56], in which only a few lines of data are collected to yield projections of the signal in the image domain. Finally, the reconstruction process will be implemented in a framework such as the Gadgetron [57], which utilizes GPUs to support real-time image reconstruction.

VIII. Conclusions

In this paper, a Jacobian-based inverse kinematics method for controlling an MRI-guided magnetically-actuated steerable catheter is presented. The paper evaluated the reproducibility and accuracy of the open-loop control of catheter system using this method in hardware experiments. The results demonstrated that the catheter performing four distinct geometric trajectories (lemniscate, circle, rectangle and butterfly) has very high reproducibility and fair accuracy.

This method paves the way for effective and accurate control of the robotic catheter in a closed-loop control system with feedback information from real-time MRI-guidance. The open-loop accuracy level makes it reasonable to expect that a closed-loop control system can achieve the desired 1 mm accuracy level. Closed-loop catheter control, modeling of catheter-surface contact, and heat management of the coils [47] are important challenges, which will be subjects of our future work. Currently, most surgical robotic systems (e.g., [5, 45, 46]) are operated in open-loop, relying on teleoperation of the operator using doctor-in-the-loop paradigm to steer the system relative to the anatomy. The presented Jacobian-based open-loop control scheme can also be used as part of such a doctor-in-the-loop teleoperation paradigm.

IX. Author Contributions

Conceived and designed the experiments: TL, RJ, NS, MAG, MCC. Performed the experiments: TL, RJ, DF, NLP, RKC, MCC. Prototyped catheter tools: NLP. Contributed amplifier box: RKC, RJ. Contributed camera-based vision system: TL, RJ. Analyzed the data: TL. Wrote the paper: TL, RJ, DF, MCC. Edited the video: TL, RJ.

References

[1] *What Is Catheter Ablation?*, National Heart Lung and Blood Institute, http://www.nhlbi.nih.gov/health/health-topics/topics/ablation/.

[2] J. Dewire and H. Calkins, "State-of-the-art and emerging technologies for atrial fibrillation ablation," *Nat. Rev. Cardiol.*, vol. 7, pp. 129–138, 2010.

[3] T. Liu and M. C. Cavusoglu, "Three dimensional modeling of an MRI actuated steerable catheter system," in *Proc. IEEE Int. Conf. Robot. Autom.*, May 2014, pp. 4393–4398.

[4] *Niobe® ES Magnetic Navigation System*, Stereotaxis, http://www.stereotaxis.com/niobe.html.

[5] *Sensei® X Robotic Catheter System*, Hansen Medical, http://www.hansenmedical.com/.

[6] Y. Fu, H. Liu, W. Huang, S. Wang, and Z. Liang, "Steerable catheters in minimally invasive vascular surgery," *Int. J. Med. Robot. Comp.*, vol. 5, no. 4, pp. 381–391, 2009.

[7] S. Nazarian, A. Kolandaivelu, M. M. Zviman, G. R. Meininger, R. Kato, R. C. Susil, A. Roguin, T. L. Dickfeld, H. Ashikaga, H. Calkins, R. D. Berger, D. A. Bluemke, A. C. Lardo, and H. R. Halperin, "Feasibility of Real-Time Magnetic Resonance Imaging for Catheter Guidance in Electrophysiology Studies," *Circulation*, vol. 118, no. 3, pp. 223–229, Jul. 2008.

[8] S. Schalla, M. Saeed, C. B. Higgins, A. Martin, O. Weber, and P. Moore, "Magnetic resonance–guided cardiac catheterization in a swine model of atrial septal defect," *Circulation*, vol. 108, no. 15, pp. 1865–1870, 2003.

[9] G. R. Vergara, S. Vijayakumar, E. G. Kholmovski, J. J. E. Blauer, M. A. Guttman, C. Gloschat, G. Payne, K. Vij, N. W. Akoum, M. Daccarett, C. J. McGann, R. S. MacLeod, and N. F. Marrouche, "Real-time magnetic resonance imagingguided radiofrequency atrial ablation and visualization of lesion formation at 3 Tesla," *Heart Rhythm*, vol. 8, no. 2, pp. 295–303, Feb. 2011.

[10] L. Muller, M. Saeed, M. Wilson, and S. Hetts, "Remote control catheter navigation: options for guidance under MRI," *J. Cardiovasc. Magn. Reson.*, vol. 14, no. 1, p. 33, 2012.

[11] T. P. L. Roberts, W. V. Hassenzahl, S. W. Hetts, and R. L. Arenson, "Remote control of catheter tip deflection: An opportunity for interventional MRI," *Magn. Reson. Med.*, vol. 48, no. 6, pp. 1091–1095, 2002.

[12] F. Settecase, M. S. Sussman, M. W. Wilson, S. Hetts, R. L. Arenson, V. Malba, A. F. Bernhardt, W. Kucharczyk, and T. P. L. Roberts, "Magnetically-assisted remote control (MARC) steering of endovascular catheters for interventional MRI: a model for deflection and design implications," *Med. Phys.*, vol. 34, no. 8, pp. 3135–3142, August 2007.

[13] N. Gudino, J. A. Heilman, J. J. Derakhshan, J. L. Sunshine, J. L. Duerk, and M. A. Griswold, "Control of intravascular catheters using an array of active steering coils," *Med. Phys.*, vol. 38, no. 7, pp. 4215–4224, 2011.

[14] R. S. Sincic, C. J. Caton, P. Lillaney, S. Goodfriend, J. Ni, A. J. Martin, A. D. Losey, N. Shah, E. J. Yee, L. Evans, V. Malba, A. F. Bernhardt, F. Settecase, D. L. Cooke, M. Saeed, M. W. Wilson, and S. W. Hetts, "System architecture for a magnetically guided endovascular microcatheter," *Biomed. Microdevices*, vol. 16, no. 1, pp. 97–106, 2014.

[15] V. Lalande, F. P. Gosselin, and S. Martel, "Catheter steering using a magnetic resonance imaging system," in *Conf. Proc. IEEE Eng. Med. Biol. Soc.*, Aug. 31 - Sep. 4 2010.

[16] F. Ullrich, S. Schuerle, R. Pieters, A. Dishy, S. Michels, and B. J. Nelson, "Automated capsulorhexis based on a hybrid magnetic-mechanical actuation system," in *Proc. IEEE Int. Conf. Robot. Autom.*, May 2014, pp. 4387–4392.

[17] I. Tunay, "Modeling magnetic catheters in external fields," in *Engineering in Medicine and Biology Society, 2004. IEMBS '04. 26th Annual International Conference of the IEEE*, vol. 1, Sept 2004, pp. 2006–2009.

[18] M. N. Faddis, W. Blume, J. Finney, A. Hall, J. Rauch, J. Sell, K. T. Bae, M. Talcott, and B. Lindsay, "Novel, magnetically guided catheter for endocardial mapping and radiofrequency catheter ablation," *Circulation*, vol. 106, no. 23, pp. 2980–2985, 2002.

[19] K. Ikuta, H. Ichikawa, K. Suzuki, and D. Yajima, "Multi-degree of freedom hydraulic pressure driven safety active catheter," in *Proc. IEEE Int. Conf. Robot. Autom.*, May 2006, pp. 4161–4166.

[20] J. D. Burkhardt and A. Natale, "New technologies in atrial fibrillation ablation," *Circulation*, vol. 120, no. 15, pp. 1533–1541, 2009.

[21] T. Liu, N. Lombard Poirot, D. Franson, N. Seiberlich, M. Griswold, and M. Cavusoglu, "Modeling and validation of the three dimensional deflection of an mri-compatible magnetically-actuated steerable catheter," *IEEE Trans. Biomed. Eng.*, vol. PP, no. 99, pp. 1–1, 2016.

[22] J. J. More, *The Levenberg-Marquardt algorithm: Implementation and theory*. Berlin, Heidelberg: Springer Berlin Heidelberg, 1978, pp. 105–116.

[23] S. R. Buss and J.-S. Kim, "Selectively damped least squares for inverse kinematics," *J. Grap. T.*, pp. 37–49, 2004.

[24] S. R. Buss, "Introduction to inverse kinematics with jacobian transpose, pseudoinverse and damped least squares methods," Tech. Rep., 2004.

[25] J. Burgner-Kahrs, D. Rucker, and H. Choset, "Continuum robots for medical applications: A survey," *IEEE Trans. Robot.*, vol. 31, no. 6, pp. 1261–1280, Dec 2015.

[26] R. J. Webster and B. A. Jones, "Design and kinematic modeling of constant curvature continuum robots: A review," *Int. J. Robot. Res.*, 2010.

[27] S. Neppalli, M. A. Csencsits, B. A. Jones, and I. D. Walker, "Closed-form inverse kinematics for continuum manipulators," *Adv. Robotics*, vol. 23, no. 15, pp. 2077–2091, 2009.

[28] B. Siciliano, "Kinematic control of redundant robot manipulators: A tutorial," *J. Intell. Robot. Syst.*, vol. 3, no. 3, pp. 201–212, 1990.

[29] I. A. Gravagne, C. D. Rahn, and I. D. Walker, "Large deflection dynamics and control for planar continuum robots," *IEEE/ASME Trans. Mechatronics*, vol. 8, no. 2, pp. 299–307, June 2003.

[30] B. Jones and I. Walker, "Kinematics for multisection continuum robots," *IEEE Trans. Robot.*, vol. 22, no. 1, pp. 43–55, Feb 2006.

[31] ——, "Practical kinematics for real-time implementation of continuum robots," *IEEE Trans. Robot.*, vol. 22, no. 6, pp. 1087–1099, Dec 2006.

[32] D. Camarillo, C. Carlson, and J. Salisbury, "Configuration tracking for continuum manipulators with coupled tendon drive," *IEEE Trans. Robot.*, vol. 25, no. 4, pp. 798–808, Aug 2009.

[33] D. B. Camarillo, C. R. Carlson, and J. K. Salisbury, *Int. S. Expe. Robot.* Berlin, Heidelberg: Springer Berlin Heidelberg, 2009, ch. Task-Space Control of Continuum Manipulators with Coupled Tendon Drive, pp. 271–280.

[34] M. Yip and D. Camarillo, "Model-less feedback control of continuum manipulators in constrained environments," *IEEE Trans. Robot.*, vol. 30, no. 4, pp. 880–889, Aug 2014.

[35] ——, "Model-less hybrid position/force control: A minimalist approach for continuum manipulators in unknown, constrained environments," *IEEE Robot. Autom. Lett.*, vol. 1, no. 2, pp. 844–851, July 2016.

[36] M. Yip, J. Sganga, and D. Camarillo, "Autonomous control of continuum robot manipulators for complex cardiac ablation tasks," *J. Med. Robot. Rese.*, vol. 01, no. 02, 2016.

[37] I. Tunay, "Position control of catheters using magnetic fields," in *IEEE Int. Conf. Mechatronics*, June 2004, pp. 392–397.

[38] N. Simaan, K. Xu, W. Wei, A. Kapoor, P. Kazanzides, R. Taylor, and P. Flint, "Design and integration of a telerobotic system for minimally invasive surgery of the throat," *Int. J. Robot. Res.*, vol. 28, no. 9, pp. 1134–1153, 2009.

[39] A. Bajo, R. E. Goldman, and N. Simaan, "Configuration and joint feedback for enhanced performance of multi-segment continuum robots," in *Proc. IEEE Int. Conf. Robot. Autom.*, May 2011, pp. 2905–2912.

[40] P. Dupont, J. Lock, B. Itkowitz, and E. Butler, "Design and control of concentric-tube robots," *IEEE Trans. Robot.*, vol. 26, no. 2, pp. 209–225, April 2010.

[41] R. J. Webster, J. P. Swensen, J. M. Romano, and N. J. Cowan, *Int. S. Expe. Robot.* Berlin, Heidelberg: Springer Berlin Heidelberg, 2009, ch. Closed-Form Differential Kinematics for Concentric-Tube Continuum Robots with Application to Visual Servoing, pp. 485–494.

[42] D. Rucker and R. Webster, "Computing jacobians and compliance matrices for externally loaded continuum robots," in *Proc. IEEE Int. Conf. Robot. Autom.*, May 2011, pp. 945–950.

[43] R. Xu, A. Asadian, A. Naidu, and R. Patel, "Position control of concentric-tube continuum robots using a modified jacobian-based approach," in *Proc. IEEE Int. Conf. Robot. Autom.*, May 2013, pp. 5813–5818.

[44] M. Boushaki, C. Liu, and P. Poignet, "Task-space position control of concentric-tube robot with inaccurate kinematics using approximate jacobian," in *Proc. IEEE Int. Conf. Robot. Autom.*, May 2014, pp. 5877–5882.

[45] *The Amigo Remote Catheter System*, Catheter Robotics, Inc, http://www.catheterrobotics.com/.

[46] *da Vinci® Surgical System*, Intuitive Surgical Inc, http://www.intuitivesurgical.com/.

[47] T. Liu, N. L. Poirot, T. Greigarn, and M. Cavusoglu, "Design of an mri-guided magnetically-actuated steerable catheter," *ASME J. Med. Devices*, 2017.

[48] H. Wang, C. Wang, W. Chen, X. Liang, and Y. Liu, "Three-dimensional dynamics for cable-driven soft manipulator," *IEEE/ASME Trans. Mechatronics*, vol. 22, no. 1, pp. 18–28, Feb 2017.

[49] P. E. Dupont, J. Lock, B. Itkowitz, and E. Butler, "Design and control of concentric-tube robots," *IEEE Trans. Robot.*, vol. 26, no. 2, pp. 209–225, April 2010.

[50] D. C. Rucker, R. J. Webster, G. S. Chirikjian, and N. J. Cowan, "Equilibrium conformations of concentric-tube continuum robots," *Int. J. Robot. Res.*, 2010.

[51] T. Greigarn and M. C. Cavusoglu, "Pseudo-rigid-body model and kinematic analysis of mri-actuated catheters," in *Proc. IEEE Int. Conf. Robot. Autom.*, May 2015, pp. 2236–2243.

[52] S. Hetts, M. Saeed, A. Martin, L. Evans, A. Bernhardt, V. Malba, F. Settecase, L. Do, E. Yee, A. Losey, R. Sincic, P. Lillaney, S. Roy, R. Arenson, and M. Wilson, "Endovascular catheter for magnetic navigation under mr imaging guidance: Evaluation of safety in vivo at 1.5T," *AJNR Am. J. Neuroradiol.*, vol. 34, no. 11, pp. 2083–2091, 2013.

[53] R. C. Jackson, T. Liu, and M. Cavusoglu, "Catadioptric stereo tracking for three dimensional shape measurement of mri guided catheters," in *Proc. IEEE Int. Conf. Robot. Autom.*, May 2016.

[54] *Silicon-based polymer material (Silicone Rubber)*, AZO Materials, http://www.azom.com/properties.aspx?ArticleID=920.
[55] J.-H. Seppenwoolde, M. A. Viergever, and C. J. Bakker, "Passive tracking exploiting local signal conservation: The white marker phenomenon," *Magn. Reson. Med.*, vol. 50, no. 4, pp. 784–790, 2003.
[56] C. Flask, D. Elgort, E. Wong, A. Shankaranarayanan, J. Lewin, M. Wendt, and J. L. Duerk, "A method for fast 3d tracking using tuned fiducial markers and a limited projection reconstruction fisp (lpr-fisp) sequence," *J. Magn. Reson. Imaging*, vol. 14, no. 5, pp. 617–627, 2001.
[57] M. S. Hansen and T. S. Srensen, "Gadgetron: An open source framework for medical image reconstruction," *Magn. Reson. Med.*, vol. 69, no. 6, pp. 1768–1776, 2013.

Taoming Liu received the B.S. degree in Mechatronics Engineering from South China University of Technology, Guangzhou, China, in 2007, and the M.S. degree in Mechanical Engineering and the Ph.D. degree in Electrical Engineering from Case Western Reserve University, Cleveland, OH, in 2011 and 2017, respectively. His research interests include medical robotics, continuum robotics, mechatronics, and control systems.

Russell Jackson received a B.S. degree in electrical engineering and mathematics from Rose-Hulman Institute of Technology (Terre Haute, Indiana) in 2009. He completed his electrical engineering Ph.D in 2016 at Case Western Reserve University (Cleveland, Ohio). His dissertation work focused on automating surgical robots using visual guidance. He is currently a Post-Doctoral researcher at CWRU. His main research interests include computer vision, surgical automation, and commercial viability analysis of forthcoming technologies.

Nate Lombard Poirot received his B.S.E. in Mechanical and Aerospace Engineering from Case Western Reserve University (CWRU) in 2014. He is currently completing his M.S. in Mechanical Engineering at CWRU with a concentration in fluid dynamics and thermodynamics. His thesis work includes prototyping and validating/optimizing catheter prototypes via fluid and mechanical analysis. As an Ames Space Academy Alum ('15), his interests include the growing private space industry and hopes to apply his degree to this field.

Dominique Franson received the B.S. degree in Bioengineering from University of Maryland, College Park, MD, in 2010. She is currently working toward the Ph.D. degree with Department of Biomedical Engineering, Case Western Reserve University, Cleveland, OH. She was a Catheter Engineer at National Institutes of Health, Bethesda, MD, from 2010 to 2014. Her research interests include real-time and interventional Magnetic Resonance Imaging.

Reinhardt Kam Criss received the B.S.E. Degree In Computer Engineering from Case Western Reserve University (CWRU) in 2016. He developed and tested Electronics and circuit solutions to further the MRI-Catheter research project at MeRCIS Lab while at CWRU, and also participated on the CWRU Snow Joke Autonomous Snowplow Team. He works as a Field Service Engineer for MTI Inc. His interests include DIY Electronics, Vintage Auto Restoration, and Travel.

Nicole Seiberlich received her B.S. degree in Chemistry from Yale University in 2001, and Ph.D. in Physics from the University of Wuerzburg in 2008. She worked as a Postdoctoral Researcher and Instructor in Department of Radiology at University Hospitals of Cleveland (2008-2011), and is currently an Assistant Professor of Biomedical Engineering at Case Western Reserve University, with secondary appointments in Radiology and Electrical Engineering and Computer Science. Her research interests include fast Magnetic Resonance Imaging, signal processing and image reconstruction, quantitative MRI, and cardiac MRI. She is currently an Associate Editor of IEEE Transactions on Medical Imaging.

Mark A. Griswold is a Professor of Radiology, Biomedical Engineering, Electrical Engineering and Computer Science, and Physics at Case Western Reserve University. Dr. Griswold obtained his bachelor's degree from the University of Illinois Urbana-Champaign in Electrical Engineering. Following this, he moved to Harvard Medical School in 1993, where he led the MRI detector laboratory at Beth Israel Hospital. In 1999, he moved to Germany to complete his Ph.D. degree at the University of Wuerzburg in Biophysics. He joined the Case Western Reserve faculty in 2005. He is a recognized pioneer in the development of several innovative approaches for MRI. In particular, his parallel MRI methods have been translated into FDA-approved products by several MRI system manufacturers. These methods have led to almost an order of magnitude increase in MRI acquisition speed over the last decade. More recently his laboratory has focused on translating the increase in imaging speed into improved quantitative imaging, especially imaging of tissue/organ function. This has culminated in the development of Magnetic Resonance Fingerprinting that promises another order of magnitude in the speed of quantitative MRI.

M. Cenk Çavuşoğlu (S'93-M'01-SM'06) received the B.S. degree (1995) in Electrical and Electronic Engineering from the Middle East Technical University, Turkey, and the M.S. (1997) and Ph.D (2000). degrees in Electrical Engineering and Computer Sciences from the University of California, Berkeley. He is currently a Professor of Electrical Engineering and Computer Science, Biomedical Engineering, and Mechanical and Aerospace Engineering with Case Western Reserve University, Cleveland, OH. He was a Visiting Researcher with the INRIA Rhones-Alpes Research Center, Grenoble, France (1998), a Postdoctoral Researcher and Lecturer with the University of California, Berkeley (2000-2002), and a Visiting Associate Professor with Bilkent University, Turkey, (2009-2010). He is a Fellow of the American Institute for Medical and Biological Engineers. His research interests include robotics, systems and control theory, and human-machine interfaces, with emphasis on medical robotics, haptics, virtual environments, surgical simulation, and bio-system modeling and simulation. His current research involves applications of robotics and control engineering to biomedical and biologically inspired engineered systems.